ACS Photonics

Article

pubs.acs.org/journal/apchd5

Combined System for Efficient Excitation and Capture of LSP Resonances and Flexible Control of SPP Transmissions

Zhen Liao,[†] Xiaopeng Shen,[†] Bai Cao Pan,[†] Jie Zhao,[†] Yu Luo,*[,‡] and Tie Jun Cui*[,†,§]

[†]State Key Laboratory of Millimeter Waves, Department of Radio Engineering Southeast University, Nanjing 210096, China

[‡]The Photonics Institute and Centre for OptoElectronics and Biophotonics, School of Electrical and Electronic Engineering, Nanyang Technological University, Nanyang Avenue, 639798, Singapore

[§]Cooperative Innovation Centre of Terahertz Science, No. 4, Section 2, North Jianshe Road, Chengdu 610054, China

ABSTRACT: We propose a compact combined system which supports compound spoof surface resonances due to the coupling between spoof surface plasmon polaritons (SPPs) and localized surface plasmons (LSPs). The system is composed of ultrathin metallic spiral structures for discrete LSP resonances and an ultrathin corrugated metallic strip to guide continuous SPP modes. We demonstrate both theoretically and experimentally that the LSP resonances can be efficiently excited and captured by the SPP waveguide, while the SPP transmissions can be judiciously controlled by the LSP structures. The spoof SPP-LSP combined system may find potential applications in sensing and integrated photonic circuitry in the microwave and terahertz frequencies.

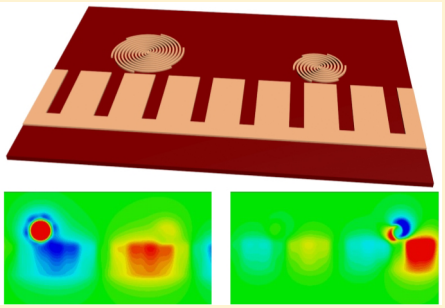

KEYWORDS: *Spoof surface plasmon, metamaterials, compound plasmon, subwavelength, sensor*

During the past decades, surface plasmons (SPs) caused by coherent electronic oscillations on the metal-dielectric interface have attracted much interests.[1] Generally speaking, SPs can be categorized into two types,[2] namely surface plasmon polaritons (SPPs) propagating along infinite metal surfaces, and localized surface plasmons (LSPs) with nonpropagating excitations of conduction electrons on finite (usually subwavelength) metallic particles.[3] Since the LSP modes strongly depend on the particle geometry, material, and environment, they have been widely used in the design of optical antennas[4,5] and sensors.[6,7] Moreover, the interplay between LSPs and SPPs in a system comprised of the coupled plasmonic structures has been studied,[8−11] and a dramatic enhancement of the electromagnetic fields resulting from the subwavelength confinement of light at small separations have been observed.[12−15]

In the microwave and terahertz frequencies, spoof (or designer) SPPs were proposed to imitate the natural SPP properties.[16−18] Recently, three-dimensional (3D) spoof SPPs called as conformal surface plasmons (CSPs) have been experimentally demonstrated.[19] CSPs are able to propagate along the edge of an ultrathin metallic structure and suffer from negligible dissipation loss. Hence, CSPs may have potential applications in plasmonic devices, circuits, and systems.[20,21] Recently, transitions between the conventional guided waves and SPP modes have been studied, which provide highly efficient methods to excite spoof SPPs.[22,23] On the other hand, two-dimensional (2D) and 3D periodically textured metallic cylinders and disks were proposed to support the electric and magnetic spoof LSPs.[24−27]

In this work, we focus on an ultrathin SPP-LSP combined system, which couples spoof SPPs to spoof LSPs efficiently at microwave frequencies. This system is comprised of subwavelength metallic spiral structures and an SPP waveguide in close proximity. We observe that the electric and magnetic LSP modes could be excited efficiently by the SPP modes, which are easily captured by measurements. Furthermore, we demonstrate that the localized features of the LSP resonances can be used to control the SPP transmissions. In order to couple electromagnetic energy into and out of the system, we design a transition section between the SPP waveguide and the conventional microstrip line. We show from both experiments and numerical simulations that the proposed system is sensitive to the refractive index of the surrounding medium. We could observe a significant frequency shift from transmission intuitively and conveniently. Using this feature, we experimentally illustrate the potential application of the proposed system as a plasmonic sensor to detect the refractive indexes of environments.

We first study an ultrathin metamaterial particle for spoof LSPs.[26] The ultrathin metallic spiral structure is shown in Figure 1a, which is composed of a small metallic disk of radius r = 2 mm surrounded by six metallic spiral arms. The arms have width w = 0.2 mm, and are separated by a distance g = 0.2 mm. The outer radius of the particle is R_1 = 3 mm. The thickness of the ultrathin metallic disk is 0.018 mm, which is based on a 0.5 mm thick dielectric substrate with the relative permittivity 2.6 and loss tangent 0.002. We consider an incoming plane wave

Received: March 4, 2015
Published: June 2, 2015

DOI: 10.1021/acsphotonics.5b00096
ACS Photonics 2015, 2, 738−743

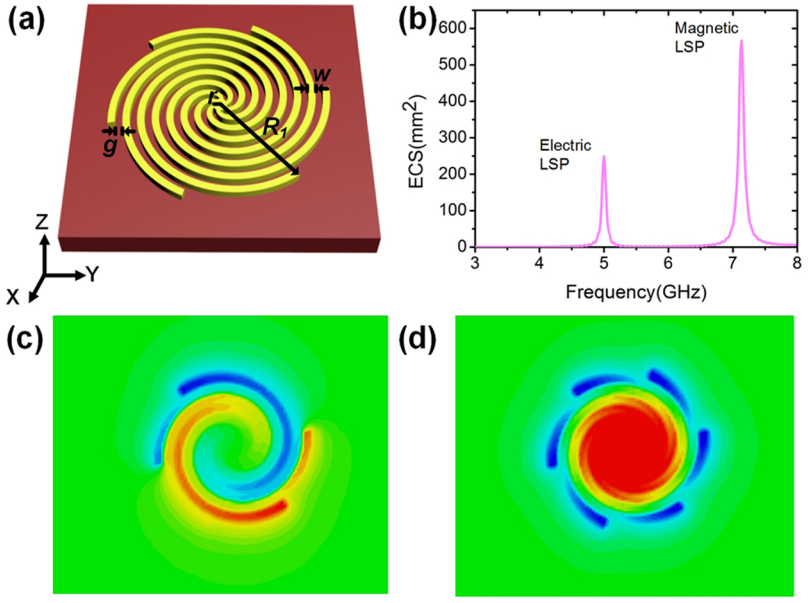

Figure 1. (a) Ultrathin spoof LSP structure, which is based on an ultrathin dielectric substrate. (b) Calculated ECS spectra of the textured metallic disk under the excitation of plane waves. (c, d) Simulation results of near-electric-field distributions corresponding to the electric and magnetic modes, which is illuminated by grazing incidence.

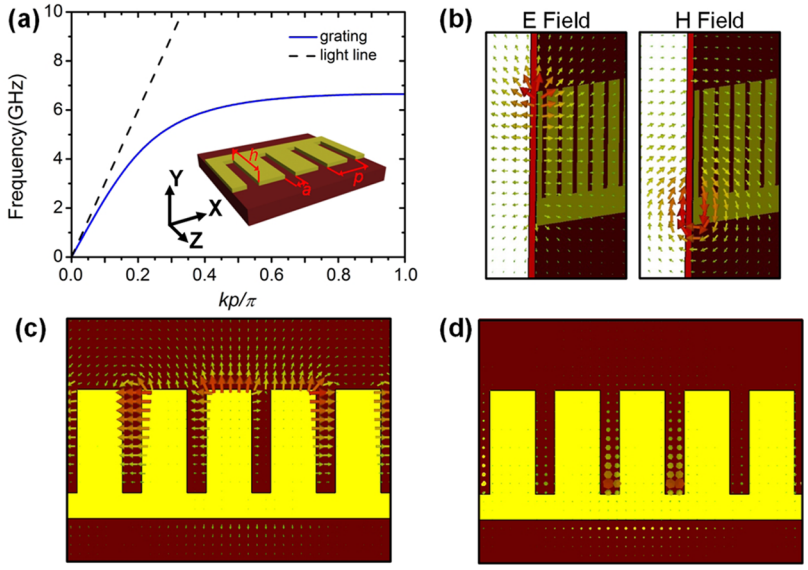

Figure 2. (a) Dispersion curve of the CSP waveguide (the blue solid line), in which the black dashed line corresponds to the light line. (b) Electric and magnetic field lines on the transverse *YZ* planes cutting the teeth. (c) Electric-field lines in the *XZ* plane. (d) Magnetic-field lines in the *XZ* plane.

propagating along the *Y* axis with the electric field polarized in the *X* direction. In Figure 1b, the extinction cross sections (ECSs) of the particle are calculated using the commercial software (CST Microwave Studio 2013), which are the sums of absorption cross sections (ACSs) and scattering cross sections (SCSs). We clearly observe that two distinct peaks occur in the ECS spectra, in which one arises from the electric mode while the other indicates the magnetic mode.

In order to verify such LSP modes, we show the *z* component of simulated electric- field patterns on an observation plane that is 0.5 mm above the disk at two resonances in Figure 1c,d, in which the red and blue colors indicate the positive and negative values, respectively. Note that the color bars in these figures and following demonstrations have been adjusted to show the mode patterns clearly. The pattern in Figure 1c presents an electric dipolar resonance at the first resonant frequency, corresponding to the natural LSP behavior. As illustrated in Figure 1d, the second peak emerges from the magnetic LSP resonance. However, the electric and magnetic resonances excited by plane waves are difficult to capture from the ECS spectra in experiments.

Then we study a SPP waveguide, in which the period, width and depth of grooves are designed as p = 5 mm, a = 1.5 mm, and h = 8 mm, respectively, as shown in the inset of Figure 2a.[19] The metallic structures have thicknesses of 0.018 mm, and supporting substrates are 0.5 mm thick. As mentioned in ref 19, the propagation constant k_p of the SPP mode is determined by the geometry of grooves. To investigate the propagation

DOI: 10.1021/acsphotonics.5b00096
ACS Photonics 2015, 2, 738−743

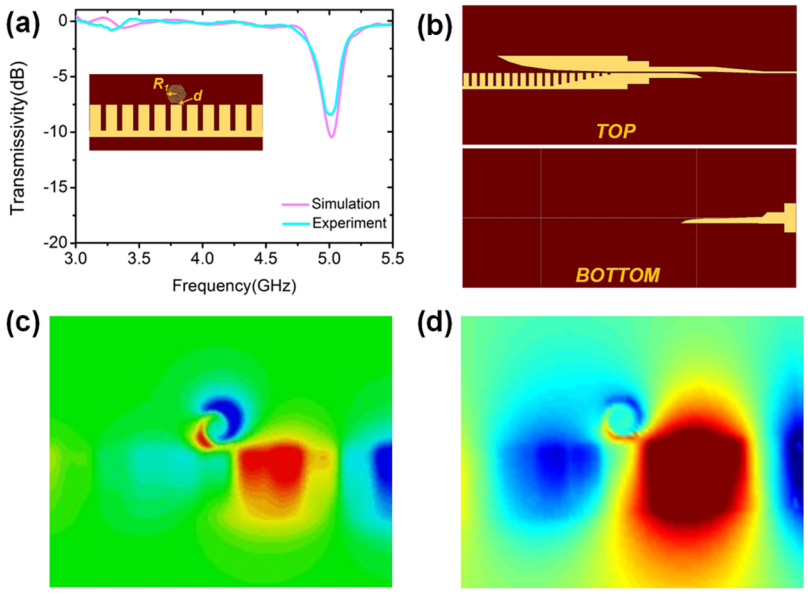

Figure 3. (a) Simulated and measured transmission coefficients of the CSP-LSP combination system with R_1 = 3 mm, in which the inset illustrates the schematic of the system. (b) Top view and bottom view of the transition. (c) Simulated E_z field distribution. (d) Measured E_z field distribution.

features of the SPP mode, we study the dispersion relation of the SPP waveguide, as shown in Figure 2a, in which the blue line is the momentum of SPPs. We clearly observe the velocity of SPPs is slower than light. That is to say, SPPs belong to the nonradiative region. However, in lower frequencies, the propagation constant k_p is close to k_0 at the light line, indicating that the waves extend over many wavelengths into the air. Therefore, the confinement of SPPs is weak. On the contrary, when the frequency approaches the asymptotic frequency, k_p is far from k_0, implying that the waves travel very slowly and are tightly confined to the corrugated metallic structure. Both conditions are not fit for the transmission of waves. Hence, we focus on the spectrum (3−5.5 GHz), which has high performance transmission. Figure 2b illustrates the electric and magnetic field vectors of SPPs in a cross section (the *YZ* plane) at 5 GHz; while Figure 2c and d shows the electric and magnetic field vectors in the *XZ* plane, respectively. From Figure 2b−d, we notice the electric field directing radially outward and the magnetic field circulating clock wise around the corrugated structure.

In the proposed SPP-LSP combined system, we place an ultrathin cooper spiral disk above the SPP waveguide in close proximity with a distance d = 0.3 mm, as illustrated in the inset of Figure 3a. The geometrical parameters are set the same as those in Figures 1a and 2a. To convert the guiding electromagnetic waves on the traditional microstrip line to the spoof SPP modes, we use a transition between the microstrip line and SPP waveguide, which has been discussed previously.[23] Figure 3b shows the top and bottom views of the transition, which could match both the momentum and impedance between the microstrip line and the SPP waveguide. Here, the geometry of the transition is optimized to obtain a high-efficiency conversion in the bandwidth from 3 to 5.5 GHz. Hence, we can connect the SPP waveguide to microstrip lines on both sides and measure the transmission coefficient of the system by using the vector network analyzers (VNAs) in experiments. As shown in Figure 3a, the experimental propagation (cyan line) of the combined system has a stop band at around 5 GHz, at which the transmission coefficient is about −10 dB, indicating that 90% energy has been blocked at this frequency.

However, the transmission coefficients in the rest frequencies are around 0 dB, indicating that the metallic spiral disk (LSP structure) has nearly no effect on SPPs, and all SPP waves can pass by the disk. From Figure 3a, the simulation and measured results are in very good agreements. We remark that all spectra are normalized with respect to the SPP waveguide without the LSP element. More importantly, the spectral position of the dip is in good agreement with the electric resonance frequency of LSPs in Figure 1a. To get a physical insight, we numerically calculate the near-electric-field (E_z) distribution at 5 GHz, as shown in Figure 3c, in which the waves are fed from the right side. It is apparent that an electric dipole LSP resonance is excited in the spiral structure. We clearly observe that the intensities of SPP modes have great differences on two sides of the LSP particle, which indicates a rejection of SPP transmission. Figure 3d illustrates the E_z field distribution in measurement, which shows reasonable agreement to the simulation. Therefore, we easily excite the electric-dipole LSP resonance using the SPP modes, which is easily captured by measuring the SPP transmission, as shown in Figure 3.

In order to reveal where the energy goes, we present experimental results on the transmission coefficient (T) and reflection coefficient (R) in Figure 4. As shown in this figure, about 17% energy transmits through the combined structure and 25% energy is reflected at the resonance frequency (∼4.9 GHz). This indicates that the electric resonance supported by the combined structure traps the energy, thereby greatly suppressing the transmission of spoof SPPs. The trapped energy is then dissipated by the absorption from the substrate and radiation to the far fields.

To better understand the combined system, we consider the other ultrathin spiral particle with radius R_2 = 4.3 mm, as shown in the inset of Figure 5a. In this case, the ECS spectrum under grazing incidence is given in Figure 5a, from which two peaks are found, indicating the electric and magnetic resonances. When the particle and SPP waveguide are put together with a gap 0.3 mm, we notice that the transmission coefficient of the

DOI: 10.1021/acsphotonics.5b00096
ACS Photonics 2015, 2, 738−743

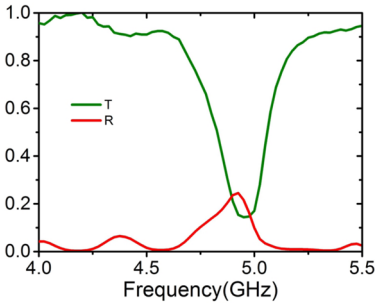

Figure 4. Measurement results of the transmission coefficient (T) and reflection coefficient (R) of the combined system.

system has a dip at around 3.65 GHz in both simulation and measurement, as illustrated in Figure 5b. The transmission is about −4.8 dB, which means that 67% energy has been rejected by the ultrathin disk at 3.65 GHz. Figure 5c,d illustrates the comparisons of E_z field distributions between simulation and measurement at the rejection frequency, showing the reasonable agreement. It is apparent that the magnetic resonance occurs in the metallic disk. And the rejection frequency of the system is equal to the magnetic LSP resonance frequency. Hence, it is evident that magnetic LSP resonance is excited by the SPP modes, and LSPs could control the SPP transmissions. Compared to the case of R_1 = 3 mm, the transmission here is higher at the rejection frequency since the magnetic LSP resonance occurring in the bigger disk (R_2 = 4.3 mm) is weaker than the electric LSP resonance in the smaller disk (R_1 = 3 mm).

To confirm the insulation of spoof LSPs in the system, we place two differently sized metallic disks (R_1 = 3 mm and R_2 = 4.3 mm) near the SPP waveguide, as shown in the inset of Figure 6a. From the simulated transmission coefficients of the system illustrated in Figure 6a, we observe dual-frequency rejections at 3.65 and 5 GHz, corresponding to the magnetic and electric LSP resonances. Such two dips are consistent with the rejection frequencies of single disks, indicating that there is nearly no interaction between two disks in the dual-disk system. The normalized experimental transmission coefficients are given in Figure 6b, which have good agreements to numerical simulations. In order to exhibit an intuitionistic view, we display the simulated E_z field distributions of the system at two rejection frequencies in Figure 6c,e. At the first rejection frequency (3.65 GHz), we notice that magnetic LSP resonance occurs on the left disk, while the fields are nearly unchanged through the right disk. In contrast, at the first rejection frequency (5 GHz), the SPP fields are cut off on the right disk due to the electric resonance, while the left disk has no impact. Such phenomena are also confirmed by the measured near-electric fields, as illustrated in Figure 6d,f. Obviously, the SPP waveguide can excite two different LSP modes with no mutual coupling in this case. This feature makes it very convenient to realize multiple rejections of spoof SPP modes, which can be used as multifrequency SPP filter.

To study the interaction between two disks, as shown in Figure 7a, we investigate the spectral behavior of the system by varying the distance s between the two spiral structures, from 17 to 7.5 mm. The simulated transmittances are presented in Figure 7b, in which the two transmission dips associated with the two spiral structures are clearly observed. We interestingly notice that the resonance frequencies of the two modes are quite robust to the separation change. On the other hand, the magnitude of transmittance at the two resonance frequencies decreases when two disks are brought closer to each other. This phenomenon can be easily understood. The two spiral structures resonate at different frequencies, and hence their spectral behaviors are immune from the plasmonic coupling. On the other hand, the reflection of Spoof SPPs at the resonance frequency is enhanced by the presence of adjacent particle, resulting in a further decrease of the transmission dip.

As is well-known, the LSP resonances have important applications in sensing, since the spectral positions of LSP resonances depend on the dielectric environments near the structure. Spoof LSP resonances have been proved sensitive to the change of surrounding materials.[25] To illustrate the good

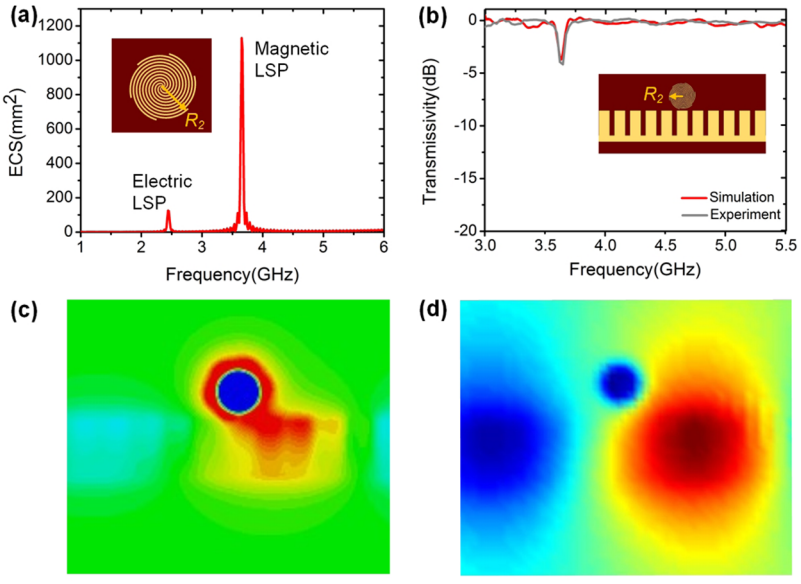

Figure 5. (a) Calculated ECS spectra of the textured metallic disk with R_2 = 4.3 mm. (b) Simulated and measured transmission coefficients of the combined system with R_2 = 4.3 mm, in which the inset indicates the schematic of the system. (c) Simulated E_z field distribution. (d) Measured E_z field distribution.

DOI: 10.1021/acsphotonics.5b00096
ACS Photonics 2015, 2, 738−743

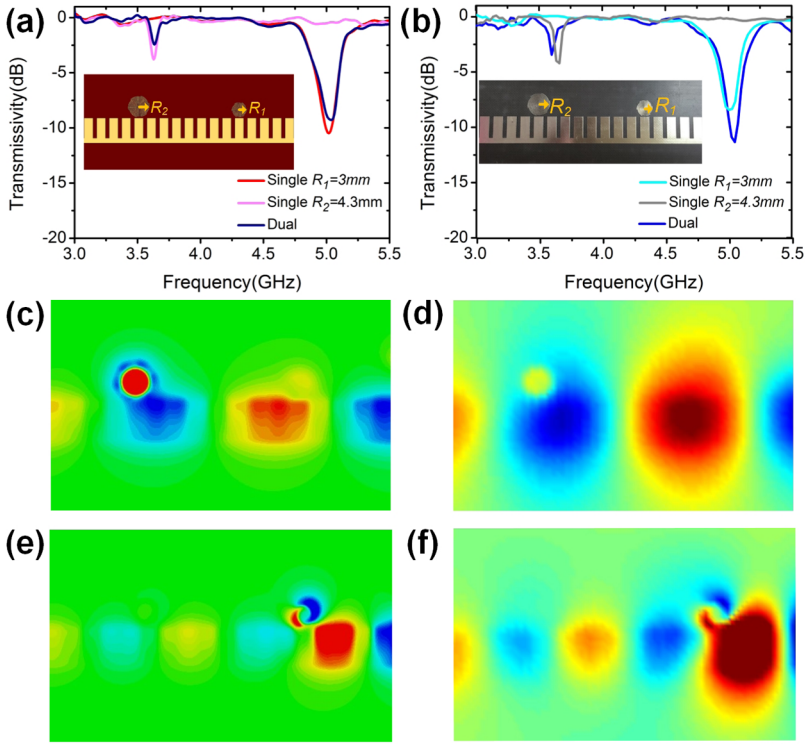

Figure 6. (a) Simulated transmission coefficients of the combined system with single-disk and dual-disk elements (see the inset for schematic). (b) Measured transmission coefficients of the combined system with single-disk and dual-disk elements (see the inset for photo). (c–f) The simulation (c, e) and measured (d, f) results of near-electric-field distributions at 3.65 and 5 GHz.

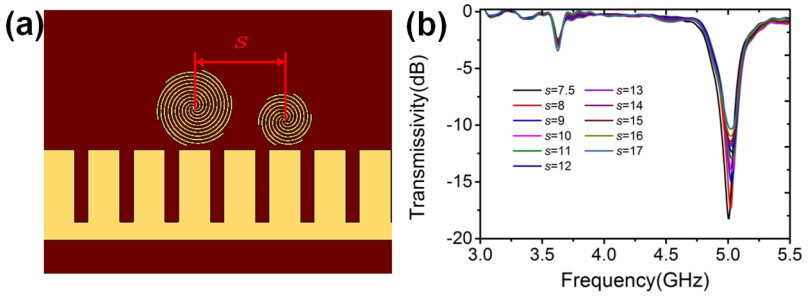

Figure 7. (a) Schematic of a combined system, in which the disks are separated with a distance *s*. (b) Simulated transmission coefficients of the combined system with different separations.

potential of the combined system as plasmonic sensor at microwave frequencies, we attach a detected dielectric sample with thickness 0.5 mm on the ultrathin metallic spiral disk (R_1 = 3 mm), as shown in the inset of Figure 8. When the refractive index of the detected material changes from 1 to 1.42, the simulation results of transmission spectra are illustrated in Figure 8, from which we observe significant shifts of rejection frequencies from 5 to 4.49 GHz. It is apparent that the higher index is detected, the lower rejection frequency is observed. We obtain a 0.51 GHz (or 10.2%) shift in the rejection frequency for a 42% change in index (from n = 1 to 1.42). Hence, the ultrathin plasmonic metamaterial system, which consists of spoof SPPs and LSPs, is a good candidate to detect the surrounding materials.

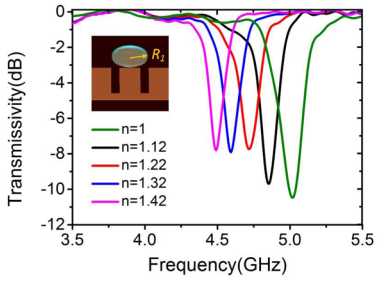

Figure 8. Simulated transmission coefficients of the combined system (see inset) surrounded by different materials.

In experiments, we put the detected sample on the ultrathin spiral disk and measure the transmission coefficients of the combined system using the vector network analyzer. The measured transmission spectra are shown in Figure 9 when the spiral disk is covered by two different materials: air and F4B dielectric pad (ε = 2.6 + i0.002) with thickness of 0.5 mm, respectively. From the measured results, we observe that the rejection frequencies have obvious shifts by covering different detected materials. We obtain 0.66 GHz shift (from 5 to 4.34 GHz) when the covering changes from air to F4B. That is to

DOI: 10.1021/acsphotonics.5b00096
ACS Photonics 2015, 2, 738–743

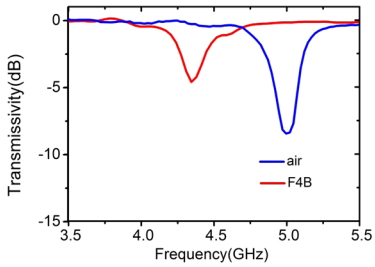

Figure 9. Measured transmission coefficients of the combined system when the LSP particle is covered by air and F4B material.

say, a 61% change of the refractive index of the detected material will result in 13.2% shift of the rejection frequencies. It is evident that the ultrathin plasmonic metamaterial system has potential applications in sensing.

In summary, we have shown an ultrathin plasmonic metamaterial system consisting of spoof SPPs and LSPs. We numerically and experimentally illustrated that both electric and magnetic LSP resonances are excited by the SPPs modes at microwave frequencies. On the other hand, the SPP transmission can be judiciously tuned by controlling the coupling strength between the two LSP particles. The property is helpful for studying the plasmonic resonances, field enhancements, and hybridizations in the future. Utilizing the LSPs resonances in the spiral disk, the transmission of SPP waves can be controlled conveniently. We also showed that the surrounding materials have significant influences on the transmission spectra in both simulations and measurements. Therefore, the proposed combined system has potential applications in plasmonic sensors and filters in the microwave and terahertz applications.

AUTHOR INFORMATION

Corresponding Authors

*E-mail: tjcui@seu.edu.cn.

*E-mail: luoyu@ntu.edu.sg.

Notes

The authors declare no competing financial interest.

ACKNOWLEDGMENTS

This work was supported by National Science Foundation of China (61171024, 61171026, and 61138001), National High Tech Projects (2012AA030402), 111 Project (111-2-05), Scientific Research Foundation of Graduate School of Southeast University (YBJJ1436), and Program for Postgraduates Research Innovation in University of Jiangsu Province (3204004910). Y.L. would like to acknowledge the funding support from NTU-A*STAR Silicon Technologies Centre of Excellence under the program Grant No. 11235150003.

REFERENCES

(1) Harvey, A. F. Periodic and Guiding Structures at Microwave Frequencies. *IRE Trans. Microwave Theory Tech.* **1960**, *8*, 30−61.

(2) Maier, S. A. *Plasmonics: Fundamentals and Applications: Fundamentals and Applications*; Springer Science & Business Media: New York, 2007.

(3) Kreibig, U.; Vollmer, M. *Optical Properties of Metal Clusters*; Springer-Verlag: New York, 1995.

(4) Mühlschlegel, P.; Eisler, H.-J.; Martin, O. J. F.; Hecht, B.; Pohl, D. W. Resonant Optical Antennas. *Science* **2005**, *308*, 1607−1609.

(5) Crozier, K. B.; Sundaramurthy, A.; Kino, G. S.; Quate, C. F. Optical Antennas: Resonators for Local Field Enhancement. *J. Appl. Phys.* **2003**, *94*, 4632−4642.

(6) Anker, J. N.; Hall, W. P.; Lyandres, O.; Shah, N. C.; Zhao, J.; Van Duyne, R. P. Biosensing with Plasmonic Nanosensors. *Nat. Mater.* **2008**, *7*, 442−453.

(7) Larsson, E. M.; Alegret, J.; Käll, M.; Sutherland, D. S. Sensing Characteristics of NIR Localized Surface Plasmon Resonances in Gold Nanorings for Application as Ultrasensitive Biosensors. *Nano Lett.* **2007**, *7*, 1256−1263.

(8) Holland, W.; Hall, D. Frequency Shifts of an Electric-Dipole Resonance near a Conducting Surface. *Phys. Rev. Lett.* **1984**, *52*, 1041−1044.

(9) Chance, R.; Prock, A.; Silbey, R. Frequency Shifts of an Electric-Dipole Transition near a Partially Reflecting Surface. *Phys. Rev. A* **1975**, *12*, 1448−1452.

(10) Lévêque, G.; Martin, O. J. F. Optical Interactions in a Plasmonic Particle Coupled to a Metallic Film. *Opt. Express* **2006**, *14*, 9971.

(11) Martín-Cano, D.; Martin-Moreno, L.; Garcia-Vidal, F. J.; Moreno, E. Resonance Energy Transfer and Superradiance Mediated by Plasmonic Nanowaveguides. *Nano Lett.* **2010**, *10*, 3129−3134.

(12) Luo, Y.; Lei, D. Y.; Maier, S. A.; Pendry, J. B. Broadband Light Harvesting Nanostructures Robust to Edge Bluntness. *Phys. Rev. Lett.* **2012**, *108*, 023901.

(13) Pendry, J. B.; Fernandez-Dominguez, A. I.; Luo, Y.; Zhao, R. Capturing Photons with Transformation Optics. *Nat. Phys.* **2013**, *9*, 518−522.

(14) Luo, Y.; Zhao, R.; Pendry, J. B. van der Waals Interactions at the Nanoscale: The Effects of Non-Locality. *Proc. Natl. Acad. Sci. U.S.A.* **2014**, *111*, 18422−18427.

(15) Pendry, J. B.; Luo, Y.; Zhao, R. Transforming the Optical Landscape. *Science* **2015**, *348*, 521−524.

(16) Garcia-Vidal, F. J.; Martín-Moreno, L.; Pendry, J. B. Surfaces with Holes in Them: New Plasmonic Metamaterials. *J. Opt. Pure Appl. Opt.* **2005**, *7*, S97.

(17) Pendry, J. B.; Martín-Moreno, L.; Garcia-Vidal, F. J. Mimicking Surface Plasmons with Structured Surfaces. *Science* **2004**, *305*, 847−848.

(18) Hibbins, A. P.; Evans, B. R.; Sambles, J. R. Experimental Verification of Designer Surface Plasmons. *Science* **2005**, *308*, 670−672.

(19) Shen, X.; Cui, T. J.; Martin-Cano, D.; Garcia-Vidal, F. J. Conformal Surface Plasmons Propagating on Ultrathin and Flexible Films. *Proc. Natl. Acad. Sci. U.S.A.* **2013**, *110*, 40−45.

(20) Gao, X.; Shi, J. H.; Shen, X.; Ma, H. F.; Jiang, W. X.; Li, L.; Cui, T. J. Ultrathin Dual-Band Surface Plasmonic Polariton Waveguide and Frequency Splitter in Microwave Frequencies. *Appl. Phys. Lett.* **2013**, *102*, 151912.

(21) Shen, X.; Cui, T. J. Planar Plasmonic Metamaterial on a Thin Film with Nearly Zero Thickness. *Appl. Phys. Lett.* **2013**, *102*, 211909.

(22) Ma, H. F.; Shen, X.; Cheng, Q.; Jiang, W. X.; Cui, T. J. Broadband and High-Efficiency Conversion from Guided Waves to Spoof Surface Plasmon Polaritons. *Laser Photonics Rev.* **2014**, *8*, 146−151.

(23) Liao, Z.; Zhao, J.; Pan, B. C.; Shen, X. P.; Cui, T. J. Broadband Transition between Microstrip Line and Conformal Surface Plasmon Waveguide. *J. Phys. Appl. Phys.* **2014**, *47*, 315103.

(24) Pors, A.; Moreno, E.; Martin-Moreno, L.; Pendry, J.; Garcia-Vidal, F. Localized Spoof Plasmons Arise while Texturing Closed Surfaces. *Phys. Rev. Lett.* **2012**, *108*, 223905.

(25) Shen, X.; Cui, T. J. Ultrathin Plasmonic Metamaterial for Spoof Localized Surface Plasmons. *Laser Photonics Rev.* **2014**, *8*, 137−145.

(26) Liao, Z.; Luo, Y.; Fernández-Domínguez, A. I.; Shen, X.; Maier, S. A.; Cui, T. J. High-Order Localized Spoof Surface Plasmon Resonances and Experimental Verifications. *Sci. Rep.* **2015**, *5*, 9590.

(27) Huidobro, P. A.; Shen, X.; Cuerda, J.; Moreno, E.; Martin-Moreno, L.; Garcia-Vidal, F. J.; Cui, T. J.; Pendry, J. B. Magnetic Localized Surface Plasmons. *Phys. Rev. X* **2014**, *4*, 021003.

DOI: 10.1021/acsphotonics.5b00096
ACS Photonics 2015, 2, 738−743